IABSE   SEMINAR on:
AIPC   «CONCRETE STRUCTURES SUBJECTED TO TRIAXIAL STRESSES»
IVBH   17th-19th MAY, 1974 - ISMES - BERGAMO (ITALY)

III-1

Constitutive Model for the Triaxial Behaviour of Concrete

Stoffmodell für das mehrachsiale Verhalten von Beton

Modèle de Constitution pour le Comportement Triaxial du Béton

K. J. WILLAM
Ph. D., Project Leader
Institut für Statik und Dynamik der
Luft- und Raumfahrtkonstruktionen
University of Stuttgart

E. P. WARNKE
Dipl. - Ing., Research Associate
Institut für Statik und Dynamik der
Luft- und Raumfahrtkonstruktionen
University of Stuttgart

SUMMARY

This paper describes different models for the failure surface and the constitutive behaviour of concrete under triaxial conditions. The study serves two objectives, the working stress design and the ultimate load analysis of three-dimensional concrete components.

In the first part a three parameter failure surface is developed for concrete subjected to triaxial loading in the tension and low compression regime. This model is subsequently refined by adding two additional parameters for describing curved meridians, thus extending the range of application to the high compression zone.

In the second part two constitutive models are formulated for elastic perfectly plastic behaviour in compression and elastic perfectly brittle behaviour in tension. Based on the normality principle, explicit expressions are developed for the inelastic deformation rate and the corresponding incremental stress-strain relation . Thus these models can be readily applied to ultimate load analysis using the initial load technique or the tangential stiffness method.

Dedicated to the 60th birthday of Professor Dr. Drs.h.c. J.H. Argyris.

1. INTRODUCTION

Over the last two decades a profound change has taken place with the appearance of digital computers and recent advances in structural analysis [1], [2], [3]. The close symbiosis between computers and structural theories was instrumental for the development of large scale finite element software packages [4] which found a wide range of application in many fields of engineering sciences.

The high degree of sophistication in structural analysis has clearly left behind many other disciplines,one of them being the field of material science. The proper description of the relevant constitutive phenomena has posed a major limitation on the analysis when applied to complex operating conditions.

In the following a constitutive model is presented for the over load and ultimate load analysis of three-dimensional concrete structures, e.g. Prestressed Concrete Reactor Vessels and Concrete Dams. Considering the size of finite elements in a typical idealization one is clearly dealing with material behaviour on the continuum level, in which the micro structure of plain and reinforced concrete components can be neglected. This scale effect of the analysis allows a macroscopic point of view according to which material phenomena such as cracking can be simulated by the behaviour of an equivalent continuum.

The objective of this study is twofold: First a mathematical model is developed for the description of initial concrete failure under triaxial conditions. Subsequently, this formulation is applied to construct a constitutive model for the over load and ultimate load analysis of three-dimensional concrete structures. Alternatively, the failure surface can be applied to working stress design using relevant safety philosophies.

In the first part a three parameter model is developed which defines a conical failure surface with non-circular base section in the principal stress space, thus the strength depends on the hydrostatic as well as deviatoric stress state. The proposed failure surface is convex, continuous and has continuous gradient directions furnishing a close fit of test data in the low compression range. In the tension regime the model may be augmented by a tension cut-off criterion. This basic formulation is refined in Appendix II by a five parameter model with curved meridians which provides a close fit of test data also in the high compression regime.

Subsequently, a material model is constructed based on an elastic perfectly plastic formulation which is augmented by a brittle failure condition in the tensile regime. In this context equivalent constitutive constraint conditions are developed, based on the "normality" principle, which can be readily applied to the finite element analysis via the concept of initial loads.

In the past considerable experimental evidence has been gathered which could be used for the construction of a triaxial failure envelope of concrete. However, most of the data were ob - tained from tests with proportional loading and uniform stress or strain conditions which were distorted by unknown boundary layer effects. For the ultimate load analysis via finite elements these two assumptions are clearly invalid. The non-linearity is responsible for local unloading even if the structure is subjected to monotonically increasing stresses. Moreover, the action of a curved thick-walled structure is controlled by non-uniform stress distributions, even if global bending effects and local stress concentrations are neglected for the time being. However, for obvious reasons it is customary to assume that test results from uniform stress- or strain experiments can be used to predict the failure behaviour of structural components subjected to non-uniform stress or strain conditions. One should be aware that this fundamental hypothesis has little justification, except that it is at present the only realistic approach for constructing a phenomenological constitutive law. The actual mechanism of crack initiation and crack propagation could in fact differ fundamentally between uniform and non-uniform stress distributions.

Considerable test data has accumulated on the multiaxial failure behaviour of mortar and concrete specimens subjected to short term loads. The experimental results can be classified into tests in which either two or three stress components are varied independently. To the first category belong the classical triaxial compression tests on cylindrical specimens (triaxial cell experiments) [5], [6], [7], [8], [9] and the biaxial tension-compression tests on hollow cylinders [10],

[11] . In addition, there is the class of biaxial compression and tension-compression tests on slabs [12], [13], [14], [15], [16], [17], [18], [19]. The second category contains experiments in which cubic specimens are subjected to arbitrary load combinations [20], [21]. Some of these types of tests are presently still being processed [22], [23], [24].

So far few attempts have been made to utilize this experimental evidence for constructing a mathematical model of the triaxial failure behaviour of concrete. A comprehensive study of this problem was undertaken in [25], for which similar conclusions were reached in [26], [27]. All three models fall into the class of pyramidal failure envelopes which have been examined extensively within the context of brittle material models as generalizations of the Mohr-Coulomb criterion [28]. In the same publication different modifications of the Griffith criterion are discussed, which have also been applied in [20] to model the failue surface of cubic mortar specimens in the tension-compression regime.

None of these previous studies on failure envelopes was directed towards the non-linear analysis of concrete structures. To this end a number of rather simple material formulations were reviewed in [29], [30], [31] and applied to the ultimate load analysis of different concrete structures.

2. TRIAXIAL FAILURE SURFACE

In the following a mathematical model is developed for the triaxial failure surface of concrete type materials. Assuming isotropic behaviour the initial failure envelope is fully described in the principal stress space.

Figure 1 shows the triaxial envelope of concrete type materials. The failure surface is basically a cone with curved meridians and a non-circular base section. The limited tension capacity is responsible for the tetrahedral shape in the tensile regime, while in compression a cylindrical form is ultimately reached.

For the mathematical model only a sextant of the principal stress space has to be considered, if the stress components are ordered according to $\sigma_1 \geqslant \sigma_2 \geqslant \sigma_3$. The surface is conveniently represented by hydrostatic and deviatoric sections where the first one forms a meridianal plane which contains the equisectrix $\sigma_1 = \sigma_2 = \sigma_3$ as an axis of revolution. The deviatoric section lies in a plane normal to the equisectrix, the deviatoric trace being described by the polar coordinates r, θ , see Fig. 2.

Basically, there are four aspects to the mathematical model of the failure surface:

1. Close fit of experimental data in the operating range.

2. Simple identification of model parameters from standard test data.

3. Smoothness – continuous surface with continuously varying tangent planes.

4. Convexity – monotonically curved surface without inflection points.

Close approximation of concrete data is reached if the failure surface depends on the hydrostatic as well as the deviatoric state, whereby the latter should distinguish different strength values according to the direction of deviatoric stress. Therefore, the failure envelope must be basically a conical surface with curved meridians and a non-circular base section. In addition, in the tensile regime the failure suface could be augmented by a tension cut-off criterion in the form of a pyramid with triangular section in the deviatoric plane.

Simple identification means that the mathematical model of the failure surface is defined by a very small number of parameters which can be determined from standard test data, e.g. uniaxial tension, uniaxial compression, biaxial compression tests, etc. The description of the failure surface should also encompass simple failure envelopes for specific model parameters. In other words, the cylindrical von Mises and the conical Drucker-Prager model should be special cases of the sophisticated failure formulation.

Continuity is an important property for two reasons: From a computational point of view, it is very convenient if a single description of the failure surface is valid within the stress space under consideration. From the theoretical point of view the proposed failure surface should have a unique gradient for defining the direction of the inelastic deformations according to the 'normality principle'. The actual nature of concrete failure mechanisms also supports the concept of a gradual change of strength for small variations in loading.

Geometrically, the smoothness condition implies that the failure surface is continuous and has continuous derivatives. Therefore, the deviatoric trace of the failure surface must pass through r_1 and r_2 with the tangents t_1 and t_2 at $\theta = 0°$ and $\theta = 60°$, see Fig. 2. Recall that for isotropic conditions only a sextant of the stress space has to be considered, $0 \leq \theta \leq 60°$.

Convexity is an important property since it assures stable material behaviour according to the postulate of Drucker [32], if the "normality" principle determines the direction of inelastic deformations. Stability infers positive dissipation of inelastic work during a loading cycle according to the concepts of thermodynamics . Figure 3 indicates that convexity of the overall deviatoric trace can be assured only if there are no inflection points and if the position vector satisfies the basic convexity condition

$$\frac{r_1}{r_2} > \frac{1}{2} \qquad \text{where} \qquad r_1 = r(\theta = 0°, 120°, 240°)$$

$$r_2 = r(\theta = 60°, 180°, 300°) \qquad (1)$$

Continuity infers compatibility of the position vectors and the slopes at $\theta = 0°$ and $\theta = 60°$. Consequently, there are at least four conditions for curve-fitting the deviatoric trace within $0° \leq \theta \leq 60°$. In addition, the convexity condition implies that the curve should have no inflection points in this interval, thus the approximation can not be based on trigonometric functions [30] or Hermitian interpolation. If the curve should also degenerate to a circle for $r_1 = r_2$, then an elliptic approximation has to be used for the functional variation of the deviatoric trace. The ellipsoidal surface assures smoothness and convexity for all position vectors r satisfying

$$\frac{1}{2} r_2 \leq r < r_2 \qquad (2)$$

The geometric construction of the ellipse is shown in Fig. 4, the details of the derivation are given in the Appendix I. The half axes of the ellipse a, b are defined in terms of the position vectors r_1, r_2 by

$$a^2 = \frac{r_2(r_1 - 2r_2)^2}{5r_2 - 4r_1} \qquad (3)$$

$$b = \frac{2r_1^2 - 5r_1 r_2 + 2r_2^2}{4r_1 - 5r_2}$$

The elliptic trace is expressed in terms of the polar coordinates r, θ by

$$r(\theta) = \frac{2r_2(r_2^2 - r_1^2)\cos\theta + r_2(2r_1 - r_2)\left[4(r_2^2 - r_1^2)\cos^2\theta + 5r_1^2 - 4r_1 r_2\right]^{\frac{1}{2}}}{4(r_2^2 - r_1^2)\cos^2\theta + (r_2 - 2r_1)^2} \qquad (4a)$$

with the angle of similarity θ

$$\cos\theta = \frac{\sigma_1 + \sigma_2 - 2\sigma_3}{\sqrt{2}\left[(\sigma_1 - \sigma_2)^2 + (\sigma_2 - \sigma_3)^2 + (\sigma_3 - \sigma_1)^2\right]^{\frac{1}{2}}} \qquad (4b)$$

In the following the deviatoric trace is used as base section of a conical failure surface with the equisectrix as axis of revolution. A linear variation with hydrostatic stress generates a cone with straight line meridians. In this case the failure surface is defined in principal stress space by a homogeneous expansion in the "average" stress components σ_α, τ_α and the angle of similarity θ.

$$f(\sigma) = f(\sigma_\alpha, \tau_\alpha, \theta) = \frac{1}{z} \frac{\sigma_\alpha}{f_{cu}} + \frac{1}{r(\theta)} \frac{\tau_\alpha}{f_{cu}} - 1 \tag{5}$$

The average stress components σ_α, τ_α represent the mean distribution of normal and shear stresses on an infinitesimal spherical surface. These values are normalized in the failure condition eq. (5) by the uniaxial compressive strength f_{cu}. The stress components are defined in terms of principal stresses by

$$\sigma_\alpha = \frac{1}{3}(\sigma_1 + \sigma_2 + \sigma_3)$$

$$\tau_\alpha = \frac{1}{\sqrt{15}} \left[(\sigma_1 - \sigma_2)^2 + (\sigma_2 - \sigma_3)^2 + (\sigma_3 - \sigma_1)^2 \right]^{\frac{1}{2}} \tag{6}$$

These scalar representations of the state of stress at a point are related to the stress components on the "octahedral" plane σ_0, τ_0 by

$$\sigma_\alpha = \sigma_0$$

$$\tau_\alpha = \sqrt{\frac{3}{5}} \tau_0 \tag{7a}$$

The average stress components also correspond to the first principal stress invariant I_1 and the second deviatoric stress invariant I_{D2} according to

$$\sigma_\alpha = \frac{1}{3} I_1$$

$$\tau_\alpha = \sqrt{\frac{2}{5}} I_{D2}^{\frac{1}{2}} = \sqrt{\frac{2}{15}} (I_1^2 - 3I_2)^{\frac{1}{2}} \tag{7b}$$

For material failure, $f(\sigma) = 0$, the following constraint condition must hold between the average normal stress and the average shear stress

$$\frac{\tau_\alpha}{f_{cu}} = r(\theta) \left[1 - \frac{1}{z} \frac{\sigma_\alpha}{f_{cu}} \right] \tag{8}$$

The free parameters of the failure surface model z, r_1 and r_2 are identified below from typical concrete test data, such as the uniaxial tension test f_t, the uniaxial compression test f_{cu} and the biaxial compression test f_{cb}. Introducing the strength ratios α_z, α_u

$$\alpha_z = f_t / f_{cu} \tag{9}$$

$$\alpha_u = f_{cb} / f_{cu}$$

the three tests are characterized by

TEST	σ_a/f_{cu}	τ_a/f_{cu}	θ	$r(\theta)$
$\sigma_1 = f_t$	$\frac{1}{3}\alpha_z$	$\sqrt{\frac{2}{15}}\,\alpha_z$	$0°$	r_1
$\sigma_3 = f_{cu}$	$-\frac{1}{3}$	$\sqrt{\frac{2}{15}}$	$60°$	r_2
$\sigma_2 = \sigma_3 = f_{cb}$	$-\frac{2}{3}\alpha_u$	$\sqrt{\frac{2}{15}}\,\alpha_u$	$0°$	r_1

$$(10)$$

Substituting these strength values into the failure condition eq. 8, the model parameters are readily obtained

$$z = \frac{\alpha_u\,\alpha_z}{\alpha_u - \alpha_z}$$

$$r_1 = \sqrt{\frac{6}{5}}\;\frac{\alpha_u\,\alpha_z}{2\alpha_u + \alpha_z}$$

$$r_2 = \sqrt{\frac{6}{5}}\;\frac{\alpha_u\,\alpha_z}{3\alpha_u\alpha_z + \alpha_u - \alpha_z}$$

$$(11)$$

The apex of the conical surface lies on the equisectrix at

$$\frac{\sigma_a}{f_{cu}} = z \tag{12}$$

The opening angle φ of the cone varies between

and

$$\tan\varphi_1 = -\frac{r_1}{z} \qquad\qquad \text{at} \quad \theta = 0°$$

$$\tan\varphi_2 = -\frac{r_2}{z} \qquad\qquad \text{at} \quad \theta = 60° \tag{13}$$

The proposed three parameter model is illustrated in Fig. 5 for the strength ratios $\alpha_u = 1.3$ and $\alpha_z = 0.1$. The hydrostatic and deviatoric sections indicate the convexity and smoothness of the failure envelope. The proposed failure surface degenerates to the Drucker-Prager model of a circular cone if

or

$$r_1 = r_2 = r_0 \tag{14}$$

$$\alpha_z = \frac{\alpha_u}{3\alpha_u - 2}$$

In this case the conical failure surface is described by the two parameters z and r_0

$$\frac{1}{z}\,\frac{\sigma_a}{f_{cu}} + \frac{1}{r_0}\,\frac{\tau_a}{f_{cu}} = 1 \tag{15}$$

The single parameter von Mises model is obtained, if in addition

or

$$z \to \infty$$

$$\alpha_u = 1$$

(16)

In this case the Drucker–Prager cone degenerates into a circular cylinder whose radius is defined by

$$\frac{1}{r_o} \frac{\tau_m}{f_{co}} = 1$$

(17)

with the strength ratios

$$\alpha_u = \alpha_z = 1$$

(18)

Figure 6 shows a comparison between the failure surface and experimental data reported in [21]. Close agreement can be observed in the low pressure regime for the strength ratios $\alpha_u = 1.8$ and $\alpha_z = 0.15$. In the high compression regime there is considerable disagreement mainly along the compressive branch. Therefore, the three parameter model is refined in the Appendix II by two additional parameters, extending the range of application to the high compression regime. This five parameter model establishes a failure surface with curved meridians in which the generators are approximated by second order parabolas along $\theta = 0°$ and $\theta = 60°$ with a common apex at the equisectrix, see also Fig. 11.

Figure 7 shows the biaxial failure envelope of the three parameter model for three different strength ratios $\alpha_u = 1.3$, $\alpha_z = 0.1$; $\alpha_u = 1.0$, $\alpha_z = 0.08$ and $\alpha_u = 1.8$, $\alpha_z = 0.15$. A comparison with test data from [18],[21] indicates that the shear strength is overestimated considerably because of the acute intersection with the biaxial stress plane. However, if we consider the dominant influence of the post–failure behaviour on the structural response [30], there is little reason for further refinements of the initial failure surface model.

3. CONSTITUTIVE MODEL

In the following the previous model of the failure envelope is utilized for the development of an elastic perfectly plastic material formulation in compression. The constitutive model is subsequently augmented by a tension cut–off criterion to account for cracking in the tension regime. In both cases it is assumed that the normality principle determines the direction of the inelastic deformation rates for ductile as well as brittle post failure behaviour.

3.1 Elastic Plastic Formulation

Inviscid plasticity is the classical approach for describing inelastic behaviour via incremental stress–strain relations. The constitutive model is based on two fundamental assumptions, an appropriate description of the material failure envelope and the definition of inelastic deformation rates e.g. via the normality principle.

a. Yield Condition

The yield surface serves two objectives, it distinguishes linear from non–linear and elastic from inelastic deformations. The failure envelope is defined by a scalar function of stress, $f(\sigma) = 0$, indicating plastic flow if the stress path intersects the yield surface. For concrete type of materials the yield condition can be approximated by the three parameter model shown in Fig. 5 or more accurately by the five parameter model developed in the Appendix II.

b. Flow Rule

For perfectly plastic behaviour the yield surface does not change its configuration during plastic flow, hence the stress path describes a trajectory on the initial yield surface, while

8.

the inelastic strains increase continuously. In this case the inelastic deformations do not contribute to the elastic strain energy, thus the inner product of plastic strain and elastic stress rates must be zero

$$\dot{\eta}_p^t \dot{\sigma} = 0$$

(19)[x]

In other words, the plastic strain rate must be perpendicular to the yield surface

$$\dot{\eta}_p = n \dot{\lambda}$$

(20)

where the normal n is the unit gradient vector of the yield surface

$$n = \frac{\partial f/\partial \sigma^t}{|\partial f/\partial \sigma^t|}$$

(21)

Explicit expressions of $\partial f/\partial \sigma^t$ are developed in Appendix III for different yield surfaces. The normal defines the direction of the plastic strain rate, the length of which determines the loading parameter $\dot{\lambda}$. The normality condition follows from Drucker's stability postulate which assures non-negative work dissipation during a loading cycle, also inferring convexity of the yield surface. For perfectly plastic behaviour the material stability is "indifferent" in the small, corresponding to the "neutral" loading condition for which initial yield and subsequent flow is governed by

$$f(\sigma) = 0 \qquad \text{and} \qquad \dot{f}(\sigma) = 0$$

(22)

The consistency condition implies that

$$\dot{f}(\sigma) = \frac{\partial f}{\partial \sigma} \dot{\sigma} = 0$$

(23)

This statement is clearly equivalent to the normality principle stated in eq. (19).

c. Incremental Stress-Strain Relations

In the following an elastic perfectly plastic consitutive model is derived using the previous statements and the kinematic decomposition of the total deformations

$$\gamma = \epsilon + \eta_p \qquad \text{and} \qquad \dot{\gamma} = \dot{\epsilon} + \dot{\eta}_p$$

(24)

The linear elastic material behaviour is given by the rate formulation of generalized Hooke's law

$$\dot{\sigma} = E \dot{\epsilon} = E (\dot{\gamma} - \dot{\eta}_p)$$

(25)

Substituting the stress rate into the consistency condition, eq. (23), we obtain

$$\frac{\partial f}{\partial \sigma} \dot{\sigma} = n^t E (\dot{\gamma} - \dot{\eta}_p)$$

(26)

This expression yields for the undetermined loading parameter $\dot{\lambda}$

$$n^t E (\dot{\gamma} - n \dot{\lambda}) = 0$$

(27)

and hereby

$$\dot{\lambda} = \frac{1}{n^t E n} n^t E \dot{\gamma}$$

(28)

---

x   The dot indicates the rate of change.

The plastic strain rate follows from eq. (20)

$$\dot{\eta}_p = n \dot{\lambda} = \frac{1}{n^t E n} \, n \, n^t E \, \dot{\gamma} \tag{29}$$

The incremental stress-strain relations are obtained by substituting $\dot{\eta}_p$ into the expression of the stress rate, eq. (25)

$$\dot{\sigma} = E \left(I_G - \frac{1}{n^t E n} \, n \, n^t E \right) \dot{\gamma} \tag{30}$$

Note the linear relationship between the stress and deformation rates in eq. (30)

$$\dot{\sigma} = F \, \dot{\gamma} \tag{31}$$

The tangential material law F is defined by

$$F = E \left(I_c - \frac{1}{n^t E n} \, n \, n^t E \right) \tag{32}$$

For perfectly plastic behaviour, F depends only on the elastic properties and the instantaneous stress state via n. The second term of eq. (32) represents the degradation of the material constitution due to plastic flow.

3.2 Elastic Cracking Formulation

Small tensile strength is the predominant feature of concrete-type materials. In the following a simple constitutive model is developed for perfectly brittle behaviour in the tensile regime. In analogy to the elastic plastic formulation the elastic cracking model is based on two fundamental assumptions, a tension cut-off criterion for the prediction of cracking and an appropriate description of inelastic deformation rates e.g. via the normality principle.

a. Crack Condition

The tension cut-off criterion distinguishes elastic behaviour from brittle fracture, i.e. separation of the material constituents due to excess tension. To this end it is assumed that the scale of observation justifies a continuum approach. For concrete-type materials cracking may be predicted by the single one parameter model based on the major principal stress

$$f(\sigma) = \sigma_1 - \sigma_\ell \qquad\qquad \text{with} \quad \sigma_1 \geqslant \sigma_2 \geqslant \sigma_3 \tag{33}$$

where σ_ℓ corresponds in general to the uniaxial tensile strength f_t. The failure surface is shown in Fig. 8, which indicates the pyramidal shape and the triangular base section in the deviatoric plane. Alternatively, the tension cut-off condition could also be expressed in terms of the three parameter model of the previous section or the five parameter model developed in the Appendix II.

b. Fracture Rule

For ductile behaviour in the post failure range the inelastic deformation rate due to cracking is derived exactly along the formulation of an elastic plastic solid. The ductile post failure behaviour forms an upper bound of the actual softening behaviour [30], which may develop in concrete components due to reinforcements, dowel action and aggregate interlock.

In the following, the case of perfectly brittle post-failure behaviour is discussed, since it requires slight modifications of the previous constitutive model for an elastic perfectly plastic solid. In analogy to elasto-plasticity the inelastic deformations due to cracking η_c do not contribute to the elastic strain energy

$$\dot{\eta}_c^t \, \dot{\sigma} = 0 \tag{34}$$

10.

This normality principle corresponds to the flow rule of plasticity stating that the inelastic strain rate due to cracking is perpendicular to the plane of fracture

$$\dot{\eta}_c = n \, \dot{\lambda} \tag{35}$$

For the maximum stress tension cut-off criterion the normal vector n is defined by the direction of the major principal stress; thus in the principal stress space

$$n = \frac{\partial f / \partial \mathbf{\sigma}^t}{|\partial f / \partial \mathbf{\sigma}^t|} = \mathbf{e}_1 \tag{36}$$

where $\mathbf{e}_1$ is the unit vector

$$\mathbf{e}_1 = \{ 1, 0, 0, 0, 0, 0 \} \tag{37}$$

For perfectly brittle behaviour the loading parameter $\dot{\lambda}$ is determined from the softening condition

$$f(\mathbf{\sigma}) = 0 \qquad \text{and} \qquad \dot{f}(\mathbf{\sigma}) = -\dot{\sigma}_t \tag{38}$$

In this case the consistency condition infers that

$$\frac{\partial f}{\partial \mathbf{\sigma}} \dot{\mathbf{\sigma}} = -\dot{\sigma}_t \tag{39}$$

c. **Inelastic Strain Increments**

In the following an expression is derived for the inelastic deformation rates due to cracking. Substituting the stress rate expression eq. (25) into the consistency condition eq. (39)

$$\frac{\partial f}{\partial \mathbf{\sigma}} \dot{\mathbf{\sigma}} = \mathbf{e}_1^t \, \mathbf{E} \, (\dot{\gamma} - \mathbf{e}_1 \dot{\lambda}) \tag{40}$$

we obtain an expression for the undetermined loading parameter $\dot{\lambda}$

$$\mathbf{e}_1^t \, \mathbf{E} \, (\dot{\gamma} - \mathbf{e}_1 \dot{\lambda}) = -\dot{\sigma}_t \tag{41}$$

and hereby

$$\dot{\lambda} = \frac{1}{\mathbf{e}_1^t \mathbf{E} \, \mathbf{e}_1} \left(\mathbf{e}_1^t \mathbf{E} \, \dot{\gamma} + \dot{\sigma}_t \right) \tag{42}$$

Note the equivalence to the elastic plastic formulation in eq. (28) except for the release of $\dot{\sigma}_t$ due to brittle softening. The resulting inelastic fracture strain rate follows from eq. (35)

$$\dot{\eta}_c = n \dot{\lambda} = \mathbf{e}_1 \dot{\lambda} \tag{43}$$

$$\dot{\eta}_c = \frac{1}{\mathbf{e}_1^t \mathbf{E} \, \mathbf{e}_1} \left(\mathbf{e}_1 \mathbf{e}_1^t \mathbf{E} \, \dot{\gamma} + \mathbf{e}_1 \dot{\sigma}_t \right)$$

The first portion of this expression can be used to construct incremental stress-strain relations in analogy to the elastic plastic formulation, see eq. (30). This part would correspond exactly to a ductile cracking model in which the major principal stress is kept constant at the tensile strength $\sigma_1 = \sigma_t$. The corresponding tangential material law would become transversely isotropic with zero stiffness along the major principal axis. Additional cracking in other directions can be considered accordingly.

The second portion of eq. (43) represents the sudden stress release due to brittle fracture, $\dot{\sigma}_t$, which is projected onto the structural level by a single initial load step in the analysis.

3.3 Transition Problem

The previous rate formulation for elastic plastic and brittle behaviour is valid in a differential sense only. In a numerical environment clearly finite increments prevail during numerical integration of the rate equations [33], [34]. This approximation problem is magnified by the sudden transition from elastic to plastic or elastic to brittle behaviour. In the latter case the discontinuity of the process is further increased due to the immediate stress release if the failure condition has been reached. Clearly, the success of the numerical technique depends primarily on the proper treatment of the transition problem for finite increments.

Consider the most general case of a finite load step shown in Fig. 9. At the outset we assume that the stress path has reached point A for which $f(\sigma_A) < 0$ indicates an elastic state. Due to the finite load increment a fully elastic stress path would reach point B penetrating the yield surface at C for proportional loading. The condition $f(\sigma_B) > 0$ violates the constitutive constraint condition

$$f(\sigma) \leq 0 \tag{45}$$

and suggests two strategies for numerical implementation.

a. Proportional Penetration Method

Assuming proportional loading the load increment is subdivided into two parts, an elastic portion for the path A - C and an inelastic portion governing the behaviour after the failure surface has been reached at C. The evaluation of the penetration point C reduces to the geometric problem of intersecting a surface with a line, a task which is non-linear for curved failure envelopes. The computation of the stress trajectory on the yield surface involves the numerical integration of

$$\sigma_P = \int_{\sigma_c}^{\sigma_B} F \, d\sigma \tag{46}$$

since the tangential material law varies with the current state of stress. In addition we have to assume that the inelastic strains increase proportionally from σ_c to σ_B. In numerical calculations additional corrections are required at each iteration step to place the stress path back onto the yield surface [37].

b. Normal Penetration Method

In this scheme we assume that the elastic path reaches the yield surface at the intersection with the normal n_D. The evaluation of the foot point D reduces to the geometric problem of minimizing the distance between B and the failure envelope, see Fig. 9

$$d = (\sigma_B - \sigma_D)^t (\sigma_B - \sigma_D) \qquad \rightarrow \qquad \text{Minimum} \tag{47}$$

The extremum condition is used to determine the components of σ_D by solving the linear system of equations.

$$\frac{\partial d}{\partial \sigma_D} = 0 \tag{48}$$

subjected to the constraint condition

$$f(\sigma_D) = 0 \tag{49}$$

Note that the loading parameter $\dot{\lambda}$ is proportional to the distance d, thus the length of the inelastic deformation increment is determined from

$$\dot{\lambda} = \frac{d}{n^t E \, n} \tag{50}$$

12.

where the normal is defined by the stress at point D

$$n = \frac{\partial f / \partial \mathbf{\sigma}_D}{|\partial f / \partial \mathbf{\sigma}_D|} \tag{51}$$

In principle both methods are feasible, yielding stress values which satisfy the constitutive constraint condition. Both formulations distort the actual path of evolution, an effect which is reduced primarily by using smaller load increments. From the standpoint of computer application the normal penetration approach is more efficient than the proportional penetration method, since the integration of eq. (46) is avoided.

4.   CONCLUDING REMARKS

Two topics were discussed, an appropriate model for concrete failure under triaxial conditions and the ensuing constitutive law for elastic perfectly plastic behaviour in compression and elastic perfectly brittle behaviour in tension.

First a three parameter failure surface was developed providing a close fit of concrete data in the low compression regime. The mathematical model establishes a convex failure envelope which is continuous with continuous first derivatives. For application in the high compression regime the formulation was extended to a five parameter model introducing curved meridians at the hydrostatic sections $\theta = 0°$ and $\theta = 60°$.

Subsequently, those failure concepts were applied to construct a constitutive model for elastic perfectly plastic behaviour in the compression regime. An analogous formulation was developed for the elastic perfectly brittle behaviour in tension using a strain softening plasticity formulation. Both constitutive models were based on appropriate failure descriptions and the normality principle determining the direction of the inelastic deformation rates. For numerical implementation the transition problem was studied in the light of finite load increments. Two penetration methods were explored for decomposing the total deformation rate into elastic and inelastic components. The normal penetration scheme offers computational advantages, in which case the transition point is determined by the intersection of the normal with the yield surface.

Some of the aspects above have been examined numerically in [30]. The unified constitutive model is presently incorporated in the finite element software system SBB which is developed at the ISD for the analysis of prestressed concrete reactor vessels [35].

At the present state there is little need for further refinements of the failure surface model. Future research should be rather directed towards the development of more sophisticated theories to trace the actual fracture mechanism under non-uniform stress conditions. Clearly, the two extreme concepts of brittle fracture and ductile yielding provide nothing but lower and upper bounds of the real behaviour in the post-failure regime and lead to a wide variation of the structural response [30]. The failure condition $f(\mathbf{\sigma}) = 0$ alone is insufficient, since the mechanism of crack propagation depends strongly on the distribution of stresses.

In addition, the normality principle should be revised since considerable dilatancy effects are introduced by the proposed model which were observed experimentally only in the vicinity of failure [24]. To this end the inelastic volumetric response could be controlled by an elliptical cap of the failure surface under hydrostatic compression [36].

APPENDICES

A I. ELLIPTIC TRACE OF FAILURE SURFACE

In the following, the curve fitting of an ellipse is briefly summarized in the deviatoric section of the failure surface. The derivation involves considerable algebra, thus only the very essential steps are indicated.

Fig. 10 shows the geometric relationships of the ellipse with x, y as principal axes. The continuity conditions of Fig. 2 imply that the minor y-axis must coincide with the position vector r_1, and the ellipse must pass through the point $P_2(m, n)$ with the normal $n(\sqrt{3}/2, 1/2)$. The half axes a, b are determined below in terms of the position vectors r_1, r_2. The standard form of an ellipse is

$$\frac{x^2}{a^2} + \frac{Y^2}{b^2} = 1 \tag{1.1}$$

Sampling this equation at the point $P_2(m, n)$ yields

$$\frac{m^2}{a^2} + \frac{n^2}{b^2} = 1 \tag{1.2}$$

Partial differentiation of eq. (1.1) establishes for the direction cosines

$$n_x = \frac{2x}{a^2} \frac{1}{R} \qquad \text{with} \qquad R = 2\left(\frac{n_x^2}{a^4} + \frac{n_y^2}{b^4}\right)^{1/2} \tag{1.3}$$

$$n_Y = \frac{2Y}{b^2} \frac{1}{R}$$

Sampling the normal at the point $P_2(m, n)$ yields for the two components

$$\frac{2m}{a^2} = R \frac{\sqrt{3}}{2} \tag{1.4}$$

$$\frac{2n}{b^2} = R \frac{1}{2}$$

These two relations form a condition for a, b

$$a^2 = \frac{m}{\sqrt{3} n} b^2 \tag{1.5}$$

The coordinates of the point P_2 are readily expressed by the position vectors r_1, r_2 and the half axis b

$$m = \frac{\sqrt{3}}{2} r_2$$

$$n = b - \left(r_1 - \frac{1}{2} r_2\right) \tag{1.6}$$

The half axes a, b are determined if we substitute eqs. (1.6) and (1.5) into eq. (1.2)

$$a^2 = \frac{r_2(r_1 - 2r_2)^2}{5r_2 - 4r_1} \tag{1.7}$$

$$b = \frac{2r_1^2 - 5r_1 r_2 + 2r_2^2}{4r_1 - 5r_2}$$

In the following the cartesian description of the ellipse is transformed into the polar coordinates r, Θ with the centroid at O. To this end we recall the polar equation of an ellipse where the pole is at the centre c', see Fig. 10

$$\varsigma^2 = \frac{a^2 b^2}{a^2 \cos^2 \varphi + b^2 \sin^2 \varphi} \tag{1.8}$$

The transformation of the ς, φ -coordinates into r, Θ follows from trigonometric relations and properties of the triangle c, c', P

$$\frac{\varsigma}{\sin \Theta} = \frac{r}{\sin \varphi} = \frac{r_1 - b}{\sin(\varphi - \Theta)} \tag{1.9}$$

and

$$\varsigma^2 = r^2 + (r_1 - b)^2 - 2r(r_1 - b)\cos\Theta \tag{1.10}$$

Using the trigonometric relation for sums of angles, we obtain from eq. (1.9)

$$\cos\varphi = \frac{r\cos\Theta - (r_1 - b)}{\varsigma} \tag{1.11}$$

Substitution into eq. (1.8) yields for the position vector ς

$$\varsigma^2 = a^2 + \frac{b^2 - a^2}{b^2} \left[r\cos\Theta - (r_1 - b) \right]^2 \tag{1.12}$$

Equating eq. (1.10) with eq. (1.12) establishes the ellipse in terms of the polar coordinates r, Θ where $0 \leq \Theta \leq 60°$

$$r(\Theta) = \frac{a^2(r_1 - b)\cos\Theta + ab\sqrt{a^2\cos^2\Theta + 2br_1\sin^2\Theta - r_1^2\sin^2\Theta}}{a^2\cos^2\Theta + b^2\sin^2\Theta} \tag{1.13}$$

Substitution of the half axes a, b into eq. (1.13) yields the final form of $r(\Theta)$ in terms of the parameters r_1, r_2

$$r(\Theta) = \frac{2r_2(r_2^2 - r_1^2)\cos\Theta + r_2(2r_1 - r_2)\sqrt{4(r_2^2 - r_1^2)\cos^2\Theta + 5r_1^2 - 4r_1 r_2}}{4(r_2^2 - r_1^2)\cos^2\Theta + (r_2 - 2r_1)^2} \tag{1.14}$$

Note that the ellipse degenerates into a circle for $r_1 = r_2$ or equivalently $a = b$.
At the meridians $\Theta = 0°$ and $\Theta = 60°$ the position vector $r(\Theta)$ turns into r_1 and r_2.

A II. FIVE PARAMETER MODEL WITH CURVED MERIDIANS

In the following the three parameter model of Section 2 is refined by adding two additional degrees of freedom for describing curved meridians. In this way, the failure surface model can be applied to low as well as high compression regimes.

In contrast to eq. (5) the linear relationship of the average stress components is replaced by the more general failure condition

$$\hat{f}(\boldsymbol{\mathsf{G}}) = \hat{f}(\bar{\sigma}_a, \tau_a, \Theta) = \frac{1}{r(\bar{\sigma}_a, \Theta)} \frac{\tau_a}{f_{cu}} - 1 \tag{2.1}$$

In this case the constraint condition of material failure, $\hat{f}(\boldsymbol{\mathsf{G}})=0$, infers that the average shear stress is restricted to

$$\frac{\tau_a}{f_{cu}} = r(\bar{\sigma}_a, \Theta) \tag{2.2}$$

Note that τ_a is now a single function of $\bar{\sigma}_a$, Θ instead of being the product of two disjoint functions in $\bar{\sigma}_a$ and Θ, see eq. (8). As consequence, the proposed five parameter model removes the affinity of deviatoric sections which was built into the previous three parameter model.

The failure surface model is constructed by approximating the meridians at $\Theta = 0°$ and $\Theta = 60°$ by two second order parabolas which are connected by an ellipsoidal surface, the trace of which is shown in Fig. 4. The surface is defined by an extension of eq. (4a) to incorporate the dependence on the average normal stress $\bar{\sigma}_a$.

$$r(\bar{\sigma}_a, \Theta) = \frac{2 r_2 (r_2^2 - r_1^2)\cos\Theta + r_2 (2 r_1 - r_2) \sqrt{4(r_2^2 - r_1^2)\cos^2\Theta + 5 r_1^2 - 4 r_1 r_2}}{4(r_2^2 - r_1^2)\cos^2\Theta + (r_2 - 2 r_1)^2} \tag{2.3}$$

The position vectors r_1, r_2 describe the meridians at $\Theta = 0$ and $\Theta = 60°$ as functions of the average stress $\bar{\sigma}_a$

$$r_1(\bar{\sigma}_a) = a_0 + a_1 \frac{\bar{\sigma}_a}{f_{cu}} + a_2 \frac{\bar{\sigma}_a^2}{f_{cu}^2} \qquad at \quad \Theta = 0° $$

$$r_2(\bar{\sigma}_a) = b_0 + b_1 \frac{\bar{\sigma}_a}{f_{cu}} + b_2 \frac{\bar{\sigma}_a^2}{f_{cu}^2} \qquad at \quad \Theta = 60° \tag{2.4}$$

The six degrees of freedom $a_0, a_1, a_2, b_0, b_i, b_2$ are identified below from experimental data. To this end, the uniaxial tension test f_t, the uniaxial compression test f_{cu} and the biaxial compression test f_{cb} are used in addition to two strength values in the high compression regime

$$for \qquad \hat{f} = -\frac{\bar{\sigma}_a}{f_{cu}} \qquad \qquad \int_1 = \frac{\tau_a}{f_{cu}} \qquad at \quad \Theta = 0°$$

$$\int_2 = \frac{\tau_a}{f_{cu}} \qquad at \quad \Theta = 60° \tag{2.5}$$

Moreover, the two parabolas have to pass through a common apex $\bar{\sigma}_a$ at the equisectrix, thus imposing an additional constraint condition

$$for \qquad \hat{f}_0 = \frac{\bar{\sigma}_a}{f_{cu}} \qquad \qquad r_1(\hat{f}_0) - r_2(\hat{f}_0) = 0 \tag{2.6}$$

The stress states of the five tests are summarized below together with the constraint condition of the common apex.

TEST	σ_a/f_{cu}	τ_a/f_{cu}	Θ	$r(\sigma_a,\Theta)$
$\sigma_1 = f_t$	$\frac{1}{3}\alpha_t$	$\sqrt{\frac{2}{15}}\,\kappa_t$	$0°$	$r_1(\sigma_a)$
$\sigma_2 = \sigma_3 = f_{cb}$	$-\frac{2}{3}\kappa_u$	$\sqrt{\frac{2}{15}}\,\alpha_u$	$0°$	$r_1(\sigma_a)$
	$-\xi$	ς_1	$0°$	$r_1(\sigma_a)$
$\sigma_3 = f_{cu}$	$-\frac{1}{3}$	$\sqrt{\frac{2}{15}}$	$60°$	$r_2(\sigma_a)$
	$-\xi$	ς_2	$60°$	$r_2(\sigma_a)$
	ξ_0	0	$60°$	$r_2(\sigma_a)$

(2.7)

For $\Theta = 0°$ and $\Theta = 60°$ the transcendental expression of eq. (2.3) reduces to $r_1(\sigma_a), r_2(\sigma_a)$. Therefore, only test results along these meridians are used for the identification of the six parameters $a_0, a_1, a_2, b_0, b_1, b_2$, which involves the solution of a linear problem.

Substituting the first three strength values of eq. (2.7) into the failure condition eq. (2.2) establishes the parameters a_0, a_1, a_2 at the "tensile" meridian $\Theta = 0°$

$$a_0 = \frac{2}{3}\kappa_u\, a_1 - \frac{4}{9}\kappa_u^2\, a_2 + \sqrt{\frac{2}{15}}\,\kappa_u$$

$$a_1 = \frac{1}{3}(2\kappa_u - \kappa_t)a_2 + \sqrt{\frac{6}{5}}\,\frac{\kappa_t - \kappa_u}{2\kappa_u + \kappa_t}$$

(2.8)

$$a_2 = \frac{\sqrt{\frac{6}{15}}\,\varsigma(\kappa_t - \kappa_u) - \sqrt{\frac{6}{5}}\,\kappa_t\kappa_u + \varsigma_1(2\kappa_u + \alpha_t)}{(2\kappa_u + \kappa_t)\left(\varsigma^2 - \frac{2}{3}\kappa_u\varsigma + \frac{1}{3}\alpha_t\varsigma - \frac{2}{9}\kappa_t\kappa_u\right)}$$

The apex of the failure surface follows from the condition $r_1(\bar{\sigma}_a) = 0$, hence

$$a_2\,\varsigma_0^2 + a_1\,\varsigma_0 + a_0 = 0$$

$$\varsigma_0 = \frac{-a_1 - \sqrt{a_1^2 - 4a_0 a_2}}{2a_2}$$

(2.9)

Substituting the second three strength values of eq. (2.7) into the failure condition eq (2.2) establishes the parameters b_0, b_1, b_2 at the "compressive" meridian $\Theta = 60°$

$$b_c = -\xi_o b_1 - \xi_o^2 b_2$$

$$b_1 = \left(\xi + \tfrac{1}{3}\right) b_2 + \frac{\sqrt{\tfrac{6}{5}} - 3\rho_c}{3\xi - 1}$$

$$b_2 = \frac{\rho_c\left(\xi_o + \tfrac{1}{3}\right) - \sqrt{\tfrac{2}{15}}\left(\xi_o + \xi\right)}{\left(\xi + \xi_o\right)\left(\xi - \tfrac{1}{3}\right)\left(\xi_o + \tfrac{1}{3}\right)} \tag{2.10}$$

The proposed five parameter model features a smooth surface since the continuity conditions of Section 2 are incorporated in the formulation of the position vector, eq. (2.3). The surface is also convex if the model parameters satisfy the following constraints,

$$a_o > 0 \qquad \text{and} \qquad a_1 \leq 0 \ , \ a_2 \leq 0$$

and in addition
$$b_o > 0 \qquad\qquad\qquad b_1 \leq 0 \ , \ b_2 \leq 0 \tag{2.11}$$

$$\frac{r_1(\sigma_a)}{r_2(\sigma_a)} > \frac{1}{2} \tag{2.12}$$

The five parameter model is illustrated in Fig. 11 where it is compared with experimental data reported in [21]. Close agreement can be observed for hydrostatic as well as for deviatoric sections. In the low compression regime the surface strongly resembles a tetrahedron, the planes of which bulge with increasing hydrostatic compression approximating asymptotically a circular cone.

In summary, the proposed five parameter model reproduces the principal features of the triaxial failure surface of concrete: It consists of a conical shape with curved meridians and non-circular base sections as well as non-affine sections in the deviatoric plane. The five parameter model is readily adjusted to fit a variety of simpler failure conditions:

The von Mises model is obtained if

$$a_o = b_o \qquad\qquad \text{and} \qquad a_1 = b_1 = a_2 = b_2 = 0 \tag{2.13}$$

The Drucker-Prager model is obtained if

$$a_o = b_o \qquad\qquad \text{and} \qquad a_2 = b_2 = 0$$
$$a_1 = b_1 \tag{2.14}$$

The three parameter model of Section 2 is obtained if

$$\frac{a_o}{b_o} = \frac{a_1}{b_1} \qquad\qquad \text{and} \qquad a_2 = b_2 = 0 \tag{2.15}$$

A corresponding four parameter model is obtained if

$$\frac{a_o}{b_o} = \frac{a_1}{b_1} = \frac{a_2}{b_2} \qquad\qquad \text{Affinity Condition} \tag{2.16}$$

Keeping the objective of the failure model in mind local deviations from test results appear rather meaningless. The main goal of the analysis is a sufficient level of confidence with regard to serviceability and limit load. The fluctuations of experimental measure - ments make it desirable that the failure model provides primarily conservative estimates of the actual strength values.

A III.   GRADIENTS OF DIFFERENT FAILURE MODELS

In Section 3 the normality principle is used to establish the direction of the inelastic deformation rate. To this end explicit expressions are developed below for the gradient directions of different classes of failure conditions.

a.   Tension Cut-off Model

The tension cut-off condition of eq. (33) is the simplest form of a fracture criterion for brittle materials. It predicts failure if the major principal stress reaches a limiting value

$$f(\sigma_1) = \sigma_1 - \sigma_t \tag{3.1}$$

Normally σ_t corresponds to the uniaxial tensile strength, f_t . In the case of the maximum stress criterion the gradient direction is collinear with the unit vector e_1 ,

$$\frac{\partial f}{\partial \sigma}^t = \frac{\partial f}{\partial \sigma_1} \frac{\partial \sigma_1}{\partial \sigma}^t = e_1 = \{1, 0, 0, 0, 0, 0\} \tag{3.2}$$

b.   Von Mises Model

The von Mises criterion is applied extensively as yield condition for metals. It predicts plastic flow if the average shear stress τ_a , eq. (6), reaches a limiting value σ_Y

$$f(\tau_a) = \tau_a - \sigma_Y \tag{3.3}$$

Normally σ_Y corresponds to the uniaxial strength $\sigma_Y = r_o f_{cu}$, eq. 17, or an equivalent shear strength value . The gradient is in this case collinear with the direction of the deviatoric stress

$$\frac{\partial f}{\partial \sigma}^t = \frac{\partial f}{\partial \tau_a} \frac{\partial \tau_a}{\partial \sigma}^t = \frac{1}{10\, \tau_a} \cdot \sigma_D \tag{3.4}$$

which is defined by

$$\sigma_D = \frac{1}{3} \{2\sigma_1 - \sigma_2 - \sigma_3, \; 2\sigma_2 - \sigma_3 - \sigma_1, \; 2\sigma_3 - \sigma_1 - \sigma_3, \; 0, 0, 0\} \tag{3.5}$$

c.   Drucker-Prager Model

The Drucker-Prager criterion is often applied as yield condition for rocks and soils. It predicts failure if the average stresses σ_a, τ_a, satisfy the constraint condition eq. (15)

$$f(\sigma_a, \tau_a) = \frac{1}{z}\frac{\sigma_a}{f_{cu}} + \frac{1}{r_o}\frac{\tau_a}{f_{cu}} - 1 \tag{3.6}$$

The gradient has in this case hydrostatic as well as deviatoric components. From the chainrule of differentiation we obtain

$$\frac{\partial f}{\partial \sigma}^t = \frac{\partial f}{\partial \sigma_a}\frac{\partial \sigma_a}{\partial \sigma}^t + \frac{\partial f}{\partial \tau_a}\frac{\partial \tau_a}{\partial \sigma}^t \tag{3.7}$$

The hydrostatic contribution follows from the first term

$$\frac{\partial f}{\partial \sigma_a}\frac{\partial \sigma_a}{\partial \sigma}^t = \frac{1}{z\, f_{cu}}\frac{1}{3}\, e_3 \tag{3.8}$$

with

$$e_3 = \{1, 1, 1, 0, 0, 0\}$$

The deviatoric contribution follows from the second term

$$\frac{\partial f}{\partial \tau_\alpha} \frac{\partial \tau_\alpha}{\partial \sigma^t} = \frac{1}{r_0 f_{cu}} \frac{1}{10\,\tau_\alpha} \, \mathbf{S}_D \tag{3.9}$$

The deviatoric stress $\mathbf{S}_D$ is defined in eq. (3.5).

d. Three Parameter Model

The three parameter model of Section 2 applies to concrete type materials. It predicts failure if the average stresses $\sigma_\alpha, \tau_\alpha$ and the angle of similarity θ satisfy the constraint condition eq. (5)

$$f(\sigma_\alpha, \tau_\alpha, \theta) = \frac{1}{2} \frac{\sigma_\alpha}{f_{cu}} + \frac{1}{r(\theta)} \frac{\tau_\alpha}{f_{cu}} - 1 \tag{3.10}$$

The position vector $r(\theta)$ is given in eq. (4a), thus the gradient direction has three contributions according to the chainrule of differentiation

$$\frac{\partial f}{\partial \sigma^t} = \frac{\partial f}{\partial \sigma_\alpha} \frac{\partial \sigma_\alpha}{\partial \sigma^t} + \frac{\partial f}{\partial \tau_\alpha} \frac{\partial \tau_\alpha}{\partial \sigma^t} + \frac{\partial f}{\partial \theta} \frac{\partial \theta}{\partial \sigma^t} \tag{3.11}$$

The hydrostatic component corresponds to that of the Drucker-Prager model

$$\frac{\partial f}{\partial \sigma_\alpha} \frac{\partial \sigma_\alpha}{\partial \sigma^t} = \frac{1}{2 f_{cu}} \frac{1}{3} \, \mathbf{e}_3 \tag{3.12}$$

The second term is equivalent to the deviatoric component of the Drucker-Prager model

$$\frac{\partial f}{\partial \tau_\alpha} \frac{\partial \tau_\alpha}{\partial \sigma^t} = \frac{1}{r(\theta) f_{cu}} \frac{1}{10\,\tau_\alpha} \, \mathbf{S}_D \tag{3.13}$$

Another contribution in the deviatoric section follows from the third term of eq. (3.11) which expands into

$$\frac{\partial f}{\partial \theta} \frac{\partial \theta}{\partial \sigma^t} = \frac{\partial f}{\partial v} \frac{\partial v}{\partial \theta} \frac{\partial \theta}{\partial \sigma^t} \tag{3.14}$$

The first term of eq. (3.14) follows from eq. (3.10)

$$\frac{\partial f}{\partial r} = -\frac{\tau_\alpha}{f_{cu}} \frac{1}{r^2(\theta)} \tag{3.15}$$

The second term of eq. (3.14) involves considerable manipulations because of the complex structure of $r(\theta)$, eq. (4a)

$$r(\theta) = \frac{\mu}{v} \tag{3.16}$$

where

$$\mu = 2\, v_2 (v_2^2 - v_1^2) \cos\theta + v_2 (2v_1 - v_2) \sqrt{4(v_2^2 - v_1^2)\cos^2\theta + 5v_1^2 - 4 v_1 v_2} \tag{3.17}$$

and

$$v = 4 (v_2^2 - v_1^2) \cos^2\theta + (v_2 - 2v_1)^2$$

Differentiation of eq. (3.16) yields

$$\frac{\partial r}{\partial \theta} = \frac{v \frac{d\mu}{d\theta} - \mu \frac{dv}{d\theta}}{v^2} \tag{3.18}$$

where
$$\frac{du}{d\theta} = 2\,v_2(v_1^2 - v_2^2)\,\sin\theta + \frac{4\,v_2\,(2v_1 - v_2)\,(v_1^2 - v_2^2)\,\sin\theta\cos\theta}{[4(v_1^2 - v_2^2)\cos^2\theta + 5v_1^2 - 4v_1v_2]^{\frac{1}{2}}}$$

and
$$\frac{dv}{d\theta} = 8\,(v_1^2 - v_2^2)\,\sin\theta\cos\theta \tag{3.19}$$

The third term in eq. (3.14) involves the differentiation of the angle of similarity θ, eq. (4.b)

$$\cos\theta = \frac{p}{q} \tag{3.20}$$

where

$$p = \sigma_1 + \sigma_2 - 2\sigma_3 \qquad \text{and} \qquad q = \sqrt{30}\ \tau_a \tag{3.21}$$

Differentiation with respect to stress leads to

$$\frac{\partial\theta}{\partial\sigma^t} = \frac{\partial(\cos^{-1}\frac{p}{q})}{\partial\sigma^t}$$
$$= \frac{1}{\sin\theta}\ \frac{q\,\frac{\partial p}{\partial\sigma^t} - p\,\frac{\partial q}{\partial\sigma^t}}{q^2} \tag{3.22}$$

The direction of this component is defined by

$$\frac{\partial p}{\partial\sigma^t} = \{\,1,\ 1,\ -2,\ 0,\ 0,\ 0\,\} \tag{3.23}$$

and
$$\frac{\partial q}{\partial\sigma^t} = \sqrt{\frac{6}{5}}\ \frac{1}{\tau_a}\ \sigma_D$$

The three contributions of the gradient $\partial f/\partial\sigma^t$ can now be assembled from eq. (3.12), eq. (3.13) and eq. (3.14), the terms of which are defined in eqs. (3.15), (3.18) and (3.22).

e.   Five Parameter Model
‾‾‾‾‾‾‾‾‾‾‾‾‾‾‾‾‾‾‾

In Appendix II a highly sophisticated model of the triaxial concrete failure surface was developed based on five parameters. This general formulation encompasses the other surface formulations for special values of the degrees of freedom. The five parameter model predicts failure if the state of stress satisfies the constraint condition, eq. (2.1)

$$f(\sigma_a, \tau_a, \theta) = \frac{1}{r(\sigma_a,\theta)}\ \frac{\tau_a}{f_{cu}} - 1 \tag{3.24}$$

The chainrule of differentiation yields again three contributions which determine the hydrostatic and the deviatoric components of the gradient $\partial f/\partial\sigma^t$

$$\frac{\partial f}{\partial\sigma^t} = \frac{\partial f}{\partial r}\ \frac{\partial r}{\partial\sigma_a}\ \frac{\partial\sigma_a}{\partial\sigma^t} + \frac{\partial f}{\partial r}\ \frac{\partial r}{\partial\theta}\ \frac{\partial\theta}{\partial\sigma^t} + \frac{\partial f}{\partial\tau_a}\ \frac{\partial\tau_a}{\partial\sigma^t} \tag{3.25}$$

The first term represents the hydrostatic component, the individual contributions of which are expanded below

$$\frac{\partial f}{\partial r} = -\frac{\tau_a}{f_{cu}}\ \frac{1}{r^2(\sigma_a,\theta)} \tag{3.26}$$

with
$$r(\sigma_a,\theta) = \frac{s+t}{v}$$

In contrast to eq. (3.17) s, t and v are now functions of θ as well as σ_a. From eq. (2.3)

it follows that

$$s\,(\bar{\sigma}_a,\theta) = 2\,(r_2^3 - r_1^2\,r_2)\cos\theta$$

$$t\,(\bar{\sigma}_a,\theta) = (2v_1v_2 - r_2^2)\left[4\,(r_2^2 - r_1^2)\cos^2\theta + 5r_1^2 - 4r_1 v_2\right]^{v_2}$$

and

$$v\,(\bar{\sigma}_a,\theta) = 4\,(r_2^2 - r_1^2)\cos^2\theta + (r_2 - 2v_1)^2 \tag{3.27}$$

Eq. (2.4) defines the dependence of the position vectors r_1 , r_2 on the average normal stress $\bar{\sigma}_a$.

$$r_1\,(\bar{\sigma}_a) = a_0 + a_1\,\frac{\bar{\sigma}_a}{f_{cu}} + a_2\,\frac{\bar{\sigma}_a^2}{f_{cu}^2} \tag{3.28}$$

$$r_2\,(\bar{\sigma}_a) = b_0 + b_1\,\frac{\bar{\sigma}_a}{f_{cu}} + b_2\,\frac{\bar{\sigma}_a^2}{f_{cu}^2}$$

Differentiation of $r(\bar{\sigma}_a,\theta)$ involves considerable algebra.

$$\frac{\partial r}{\partial \bar{\sigma}_a} = \frac{v\left(\frac{\partial s}{\partial \bar{\sigma}_a} + \frac{\partial t}{\partial \bar{\sigma}_a}\right) - (s+t)\frac{\partial v}{\partial \bar{\sigma}_a}}{v^2} \tag{3.29}$$

The partial derivatives with respect to the average normal stress are given by

$$\frac{\partial s}{\partial \bar{\sigma}_a} = 2\cos\theta\left[(3r_2^2 - r_1^2)dr_2 - 2v_1 v_2\,dv_1\right]$$

$$\frac{\partial t}{\partial \bar{\sigma}_a} = \left[2r_2\,dv_1 + 2(v_1 - r_2)dv_2\right]w + \frac{1}{2w}\,(2v_1 v_2 - r_2^2)\left[(-8r_1\cos^2\theta + 10v_1 - 4v_2)dv_1 + (8r_2\cos^2\theta - 4v_1)dv_2\right]$$

$$w = \left[4(r_2^2 - r_1^2)\cos^2\theta + 5r_1^2 - 4r_1 r_2\right]^{V_2} \tag{3.30}$$

and

$$\frac{\partial v}{\partial \bar{\sigma}_a} = (8r_1\sin^2\theta - 4r_2)dv_1 + (8v_2\cos^2\theta + 2r_2 - 4v_1)dv_2$$

The rate of change of the position vectors r_1 , r_2 follows from

$$dr_1 = \frac{a_1}{f_{cu}} + \frac{2a_2\,\bar{\sigma}_a}{f_{cu}^2}$$

$$dr_2 = \frac{b_1}{f_{cu}} + \frac{2b_2\,\bar{\sigma}_a}{f_{cu}^2} \tag{3.31}$$

The direction of the hydrostatic contribution is obtained in analogy to the Drucker-Prager model from eq. (3.8)

$$\frac{\partial \bar{\sigma}_a}{\partial \bar{\sigma}^t} = \frac{1}{3}\,e_3 \tag{3.32}$$

The second and third terms of eq. (3.25) define the deviatoric component of the gradient direction. These expressions correspond to the formulas derived previously for the three parameter model, eq. (3.13) and eq. (3.14), the individual contributions of which are defined in eq. (3.15), eq. (3.18) and eq. (3.22).

In conclusion, the normal n is readily determined from the gradient of the failure surface model

$$n = \frac{\partial f/\partial \bar{\sigma}^t}{|\partial f/\partial \bar{\sigma}^t|} \tag{3.33}$$

In the case of the five parameter model the normal is uniquely defined in terms of the current state of stress $\bar{\sigma}_\alpha$, τ_α and θ in addition to the six degrees of freedom a_o, a_1, a_2, b_o, b_1, b_2. The expressions for the gradient are rather elaborate, but for repeated computer applications "generality" should be the guiding axiom. To this end, the formulation of the normal for the five parameter model degenerates to the special cases of the von Mises model, the Drucker-Prager model and the three parameter model.

ZUSAMMENFASSUNG

Die vorliegende Untersuchung behandelt verschiedene dreiachsiale Modelle für die Versagensfläche und das Stoffverhalten von Beton. Zielsetzung ist die Gebrauchslast- und Grenzlastanalyse von drei-dimensionalen Betontragwerken.

Im ersten Teil wird ein drei Parametermodell entwickelt für die dreiachsiale Versagensfläche von Beton im Zug- und niedrigen Druckbereich. Für Anwendungen im hohen Druckbereich wird dieses Modell durch zwei zusätzliche Parameter erweitert, um die Krümmung in der Meridianrichtung zu erfassen.

Der zweite Teil behandelt zwei Stoffmodelle für ideal plastisches Verhalten im Druckbereich und ideal sprödes Verhalten im Zugbereich. Basierend auf dem Normalitätsprinzip werden Ausdrücke für die nicht-elastischen Verformungsänderungen und die entsprechenden inkrementellen Spannungs-Dehnungsgesetze aufbereitet, die zur Grenzlastberechnung nach dem Verfahren der Anfangslasten oder der tangentialen Steifigkeit Verwendung finden.

RÉSUMÉ

Il s'agit d'étudier différents modèles triaxiaux pour la surface de rupture et le comportement du béton. On cherche à analyser la charge de service et la charge limite de structures en béton à trois dimensions.

Dans la première partie, on développe un modèle à 3 paramètres pour la surface de rupture du béton soumis à des charges triaxiales dans le domaine de traction et de faible compression. Ce modèle est ensuite amélioré par l'introduction de deux nouveaux paramètres pour étendre le domaine d'application au cas de la haute compression (on tient ainsi compte de la courbure de la surface de rupture en direction du méridien).

Dans la seconde partie, on développe deux modèles de comportement pour le cas de comportement élastoplastique parfait en compression et élastique fragile parfait en traction. D'après le principe de normalité, on établit des expressions explicites pour les taux de déformation inélastique et pour les lois extensions- contraintes incrémentales correspondantes, qui peuvent être facilement appliquées au calcul de la charge limite en faisant appel à la technique de la charge initiale ou à la méthode de la rigidité tangentielle.

CAPTIONS OF FIGURES

Fig. 1   Initial Failure Surface of Plain Concrete under Triaxial Conditions.
Versagensfläche von Beton unter dreiachsialer Belastung.
Surface de rupture initiale du béton soumis à des charges triaxiales.

Fig. 2   Continuity of the Failure Surface.
Verträglichkeit der Versagensfläche.
Continuité de la surface de rupture.

Fig. 3   Convexity of the Failure Surface.
Konvexität der Versagensfläche.
Convexité de la surface de rupture.

Fig. 4   Elliptic Trace of Deviatoric Section for $\alpha_u = 1.3$, $\alpha_2 = 0.1$
Elliptischer Schnitt in der Deviatorebene für $\alpha_u = 1.3$, $\alpha_2 = 0.1$
Trace elliptique dans le plan du déviateur pour $\alpha_u = 1.3$, $\alpha_2 = 0.1$

Fig. 5   Three Parameter Model for $\alpha_u = 1.3$, $\alpha_2 = 0.1$
Drei Parametermodell für $\alpha_u = 1.3$, $\alpha_2 = 0.1$
Modèle à trois paramètres pour $\alpha_u = 1.3$, $\alpha_2 = 0.1$

Fig. 6   Fitting of Triaxial Test Data for Low Compression Regime.
Vergleich mit dreiachsialen Versuchsergebnissen im niederen Druckbereich.
Comparaison avec les résultats d'essais triaxiaux dans le domaine des faibles compressions.

Fig. 7   Fitting of Biaxial Test Data for Different Strength Ratios.
Vergleich mit zweiachsialen Versuchsergebnissen für verschiedene Festigkeitswerte.
Comparaison avec les résultats d'essais biaxiaux pour différentes valeurs de résistance.

Fig. 8   Maximum Tensile Stress Cut-Off Criterion.
Maximales Zugspannungskriterium.
Critère de traction maximale.

Fig. 9   Transition from Elastic into Inelastic Regime.
Übergang vom elastischen in den unelastischen Bereich.
Transition du domaine élastique au domaine inélastique.

Fig. 10   Geometric Relations of Ellipse.
Geometrische Verhältnisse der Ellipse.
Conditions géometriques de l'ellipse.

Fig. 11   Five Parameter Model for $\alpha_u = 1.8$, $\alpha_2 = 0.15$
Fünf Parametermodell für $\alpha_u = 1.8$, $\alpha_2 = 0.15$
Modèle à cinq paramètres pour $\alpha_u = 1.8$, $\alpha_2 = 0.15$
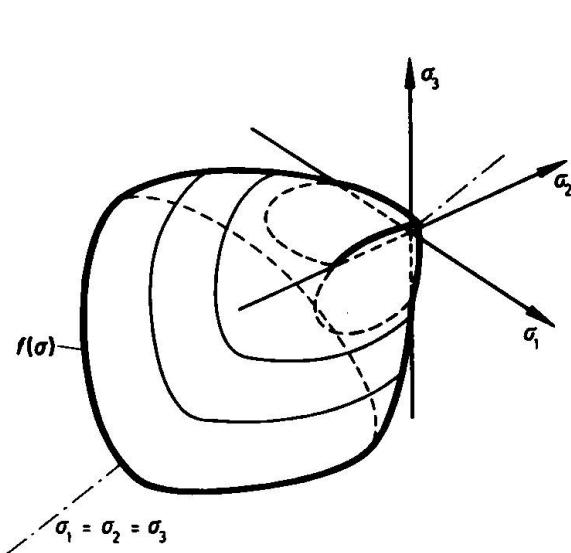
Fig.1 Initial Failure Surface
Plain Concrete under Triaxial Conditions
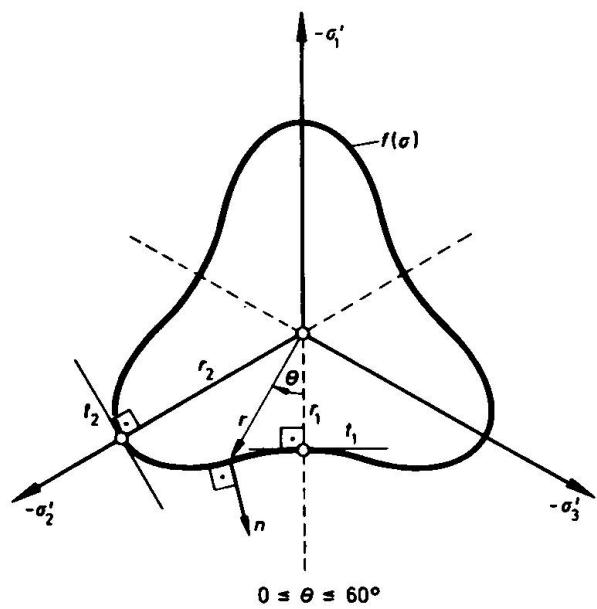
**Fig.2 Continuity of the Failure Surface**
Deviatoric Section
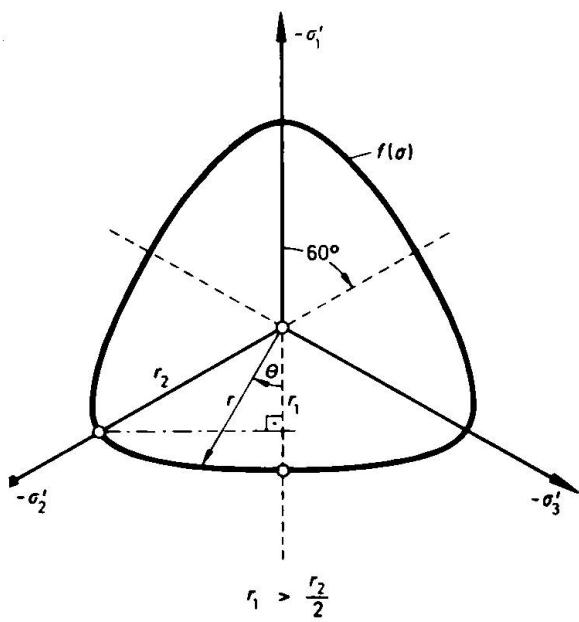
**Fig.3 Convexity of the Failure Surface**
Deviatoric Section
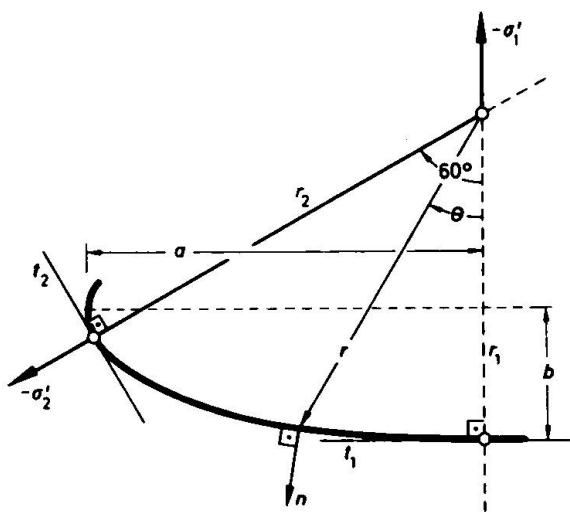
Fig.4 Elliptic Trace of the Failure Surface
Deviatoric Section for $\alpha_u = 1.3$, $\alpha_z = 0.1$

26.

Hydrostatic Section ($\theta = 0°$)

Deviatoric Section ($\sigma_a = -0.5 f_{cu}$)

$$\frac{1}{z}\frac{\sigma_a}{f_{cu}} + \frac{1}{r(\theta)}\frac{\tau_a}{f_{cu}} = 1$$
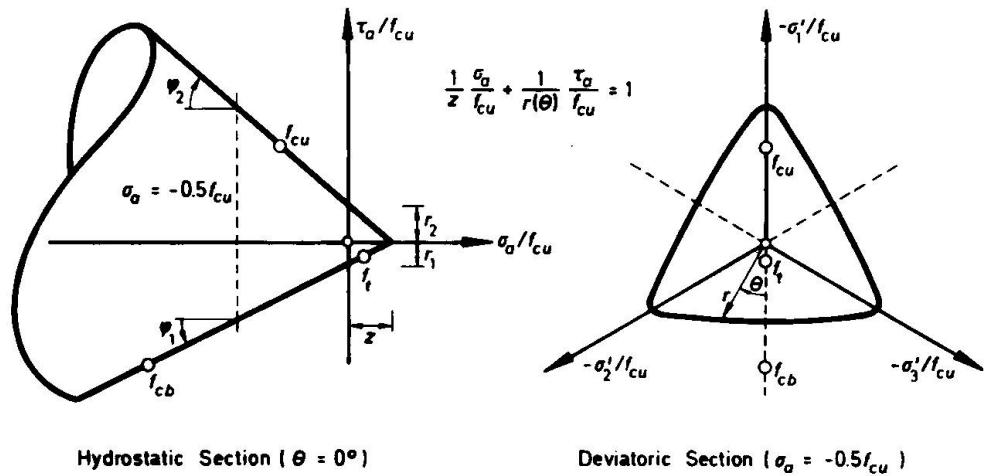
Fig.5   Three   Parameter   Model
Strength   Ratios $\alpha_u = 1.3$, $\alpha_z = 0.1$

x   Experiment (Launay et al)
—— Three Parameter Model
$\alpha_u = 1.8$, $\alpha_z = 0.15$

Hydrostatic Section ($\theta = 0$)

Deviatoric Sections ($\bar{\alpha} = 1,3,5,7$)
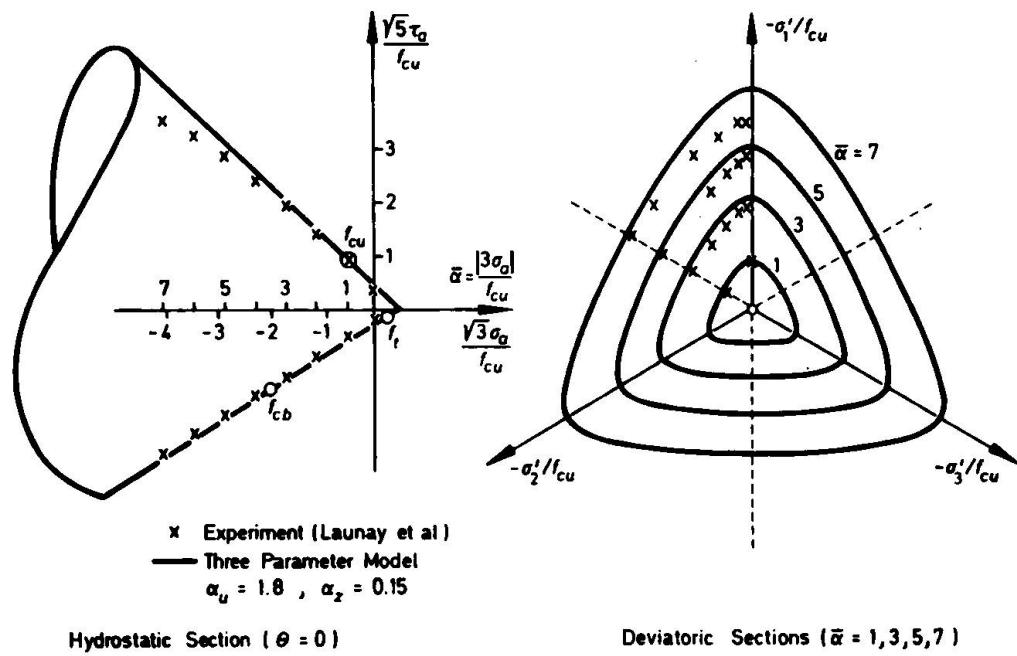
Fig.6 Fitting of Triaxial Test Data
Low Compression Regime

Experiment: + Kupfer et al
            X Launay et al

$f(\sigma)$: ——— $\alpha_u = 1.3$, $\alpha_z = 0.10$
         —·— $\alpha_u = 1.0$, $\alpha_z = 0.08$
         – – – $\alpha_u = 1.8$, $\alpha_z = 0.15$
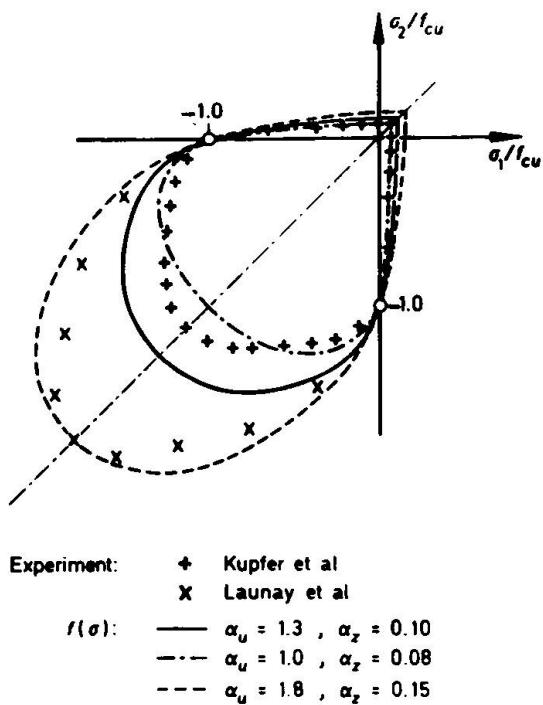
Fig.7 Fitting of Biaxial Test Data
Study of Strength Ratios

Pricipal Stress Space

Deviatoric Section
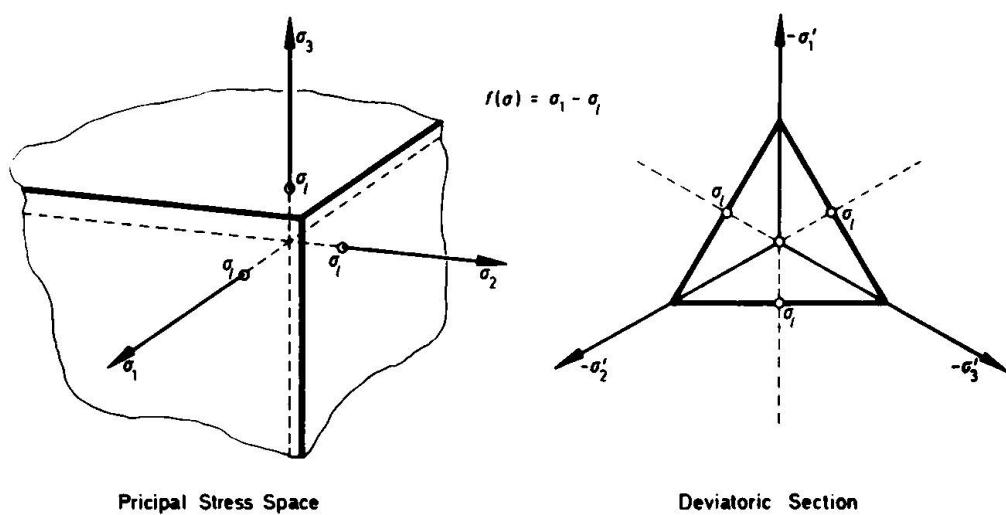
Fig.8 Tension Cut - Off Criterion
Maximum Stress Condition
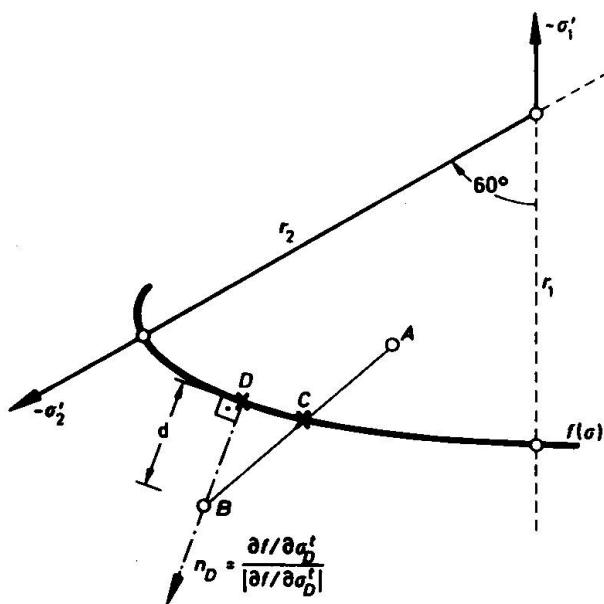
Fig.9 Transition Problem
Deviatoric Section

Fig.10 Geometric Relations of Ellipse

x Experiment (Launay et al)
——— Five Parameter Model
$\alpha_u = 1.8$, $\alpha_z = 0.15$, $\xi = 3.67$, $\vartheta_1 = 1.59$, $\vartheta_2 = 1.94$

Hydrostatic Section

Deviatoric Sections
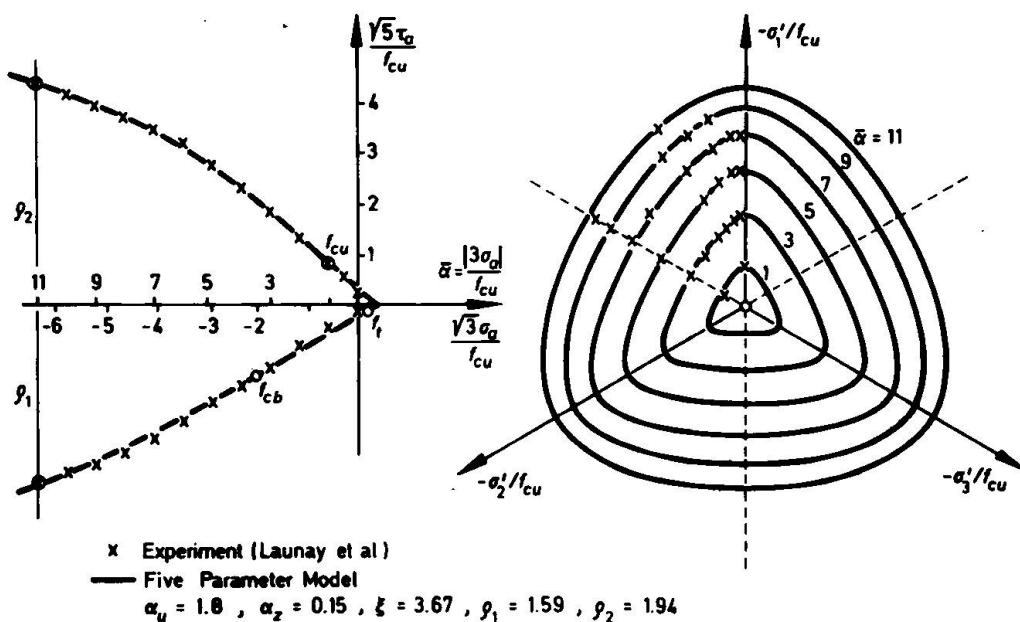
Fig.11 Five Parameter Model
Fitting of Triaxial Test Data

6. LIST OF REFERENCES

[1] J.H. ARGYRIS, Energy Theorems and Structural Analysis, Aircraft Engineering 1954-1955. Also published in book form (Butterworths, London, 1960, Third .ed. 1967).

[2] J.H. ARGYRIS, Continua and Discontinua, Opening address to 1st Int. Conf. Matrix Methods of Struct. Mechanics, Dayton, Ohio, WPAFB, 1955, published in the Proceedings by the U.S Government, January 1967.

[3] J.H. ARGYRIS, P.C. DUNNE, Some Contributions to Non-Linear Solid Mechanics, presented at IRIA, Rocquencourt, December 17-21, 1973, to be published in the Proceedings and Springer Verlag.

[4] J.H. ARGYRIS, ASKA - Automatic System for Kinematic Analysis, Nucl.Eng. and Design, Vol. 10, 1969.

[5] F.E. RICHART, A. BRANDTZAEG, R.L. BROWN, The Failure of Plain and Spirally Reinforced Concrete in Compression, University of Illinois, Eng. Expt. Stat. Bulletin No. 190, 1929.

[6] G.G. BALMER, Shearing Strength of Concrete Under High Triaxial Stress, U.S. Bureau of Reclamation, Struct. Res. Lab. Report SP-23, 1949.

[7] C.J. BELLAMY, Strength of Concrete under Combined Stresses, Proceedings ACI Vol. 58, No. 4, 1961.

[8] T.N.W. AKROYD, Concrete Under Triaxial Stress, Magazine of Concrete Research, Vol. 13, No. 39, 1961.

[9] J. CHINN, R. Zimmermann, Behaviour of Plain Concrete Under Various High Triaxial Compression Loading Conditions, U.S. Air Force Weapons Lab. Tech. Rep. WL-TR, 164-63 1965.

[10] B. BRESLER, K.S. PISTER, Strength of Concrete Under Combined Stresses, Proccedings ACI, Vol. 55, No. 3, September 1958.

[11] D. McHENRY, J. KARNI, Strength of Concrete Under Combined Tensile and Compressive Stress, Proceedings ACI, Vol. 54, No. 10, April 1958.

[12] A. FÖPPL, Mitteilung aus dem Mech. Techn. Lab. der Königl. Technischen Hochschule München, Heft 27 und 28, 1900.

[13] H. WEIGLER, G. BECKER, Untersuchungen über das Bruch- und Verformungsverhalten von Beton bei zweiachsiger Beanspruchung, Heft 157 des DAfStb., 1963.

[14] K.T.S.R. IYENGAR, K. CHANDRASHEKHARA, K.T. KRISHNASWAMY, Strength of Concrete Under Biaxial Compression, Proceedings ACI, Vol. 62, 1965.

[15] E. FUMAGALLI, Strength of Concrete Under Biaxial Compression, Proceedings ACI, Vol. 62, No. 9, September 1965.

[16] G.S. ROBINSON, Behaviour of Concrete in Biaxial Compression, Journal of the Structural Division, ASCE, Vol. 93, No. ST1, February 1967.

[17] G.W.D. VILE, Behavior of Concrete Under Short-Term Static Biaxial Stress, A.E. Brooks and K. Newman (Eds.). The Structure of Concrete, CCA London, 1968.

[18] H.B. KUPFER, H.K. HILSDORF, H. RÜSCH, Behavior of Concrete Under Biaxial Stresses, Proceedings ACI, Vol. 66, No. 8, August 1969.

[19] H.B. KUPFER, Das Verhalten des Betons unter mehrachsiger Kurzzeitbelastung unter besonderer Berücksichtigung der zweiachsigen Beanspruchung, Heft Nr. 229, DAfStb, Berlin, 1973.

[20] Y. NIWA, S. KOBAYASHI, Failure Criterion of Cement Mortar Under Triaxial Compression, Memoirs of Faculty of Engineering, Kyoto University, Japan, XXIX, 1967.

[21] P. LAUNAY, H. GACHON, Strain and Ultimate Strength of Concrete Under Triaxic Stress, ACI Special Publ. SP-34, 1972.

[22] F. BREMER, Festigkeits- und Verformungsverhalten des Betons bei mehrachsiger Beanspruchung, Beton und Stahlbetonbau, 1, 1971.

[23] G. SCHICKERT, Verformungsverhalten von Betonproben für Spannbeton Reaktordruckbehälter, 2nd Int. Conf. SMIRT, Berlin, 1973.

[24] D. LINSE, Versuchsanlage zur Ermittlung der dreiachsigen Festigkeit von Beton mit ersten Versuchsergebnissen, Cement and Concrete Research, Vol. 3, 1973.

[25] H. REIMANN, Kritische Spannungszustände des Beton bei mehrachsiger, ruhender Kurzzeitbelastung, Heft 175 des DAfStb., 1965.

[26] K. NEWMAN, J.B. NEWMAN, Failure Theories and Design Criteria for Plain Concrete, Paper 83, Symposium on Materials, Southampton, 1969.

[27] D.J. HANNANT, C.O. FREDERICK, Failure Criteria for Concrete in Compression, Magazine of Concrete Research, Vol. 20, No. 64, September 1968.

[28] B. PAUL, Macroscopic Criteria for Plastic Flow and Brittle Fracture in "Fracture, an Advanced Treatise", Vol. 2, ed. by H. Liebowitz, Acad. Press, 1968.

[29] A.C. SCORDELIS, Finite Element Analysis of Reinforced Concrete Structures, presented at Specialty Conference on the Finite Element Method in Civil Engineering, McGill University, Montreal, 1972.

[30] J.H. ARGYRIS, G. FAUST, J. SZIMMAT, E.P. WARNKE, K.J. WILLAM, Recent Developments in the Finite Element Analysis of PCRV, presented at 2nd Int. Conf. SMIRT, Berlin 1973, to appear in Nucl. Eng. and Design, Vol. 27, 1974.

[31] Z. MROZ, Mathematical Models of Inelastic Concrete Behaviour, Paper No. 2, Study No. 8 on "Inelasticity and Non-Linearity in Structural Concrete", University of Waterloo Press, 1972.

[32] D.C. DRUCKER, A Definition of Stable Inelastic Material, Journal Appl. Mech. Vol. 26, 1959.

[33] J.H. ARGYRIS, D.W. SCHARPF, Methods of Elastoplastic Analysis, Proceedings of the ISD-ISSC Symposium on Finite Element Techniques, Institut d. Statik u. Dynamik der Luft- und Raumfahrtkonstruktionen, Stuttgart, 1969 and ZAMP, 23, 1972.

[34] H. BALMER, J. DOLTSINIS, M. KÖNIG, Elastoplastic and Creep Analysis with the ASKA Program System, Computer Methods in Appl. Mech. and Eng., Vol. 3, No.1, 1974.

[35] J.H. ARGYRIS, G. FAUST, J.R. ROY, J. SZIMMAT, E.P. WARNKE, K.J. WILLA Finite Elemente zur Berechnung von Spannbeton-Reaktordruckbehältern, Heft Nr. 23 des DAfStb., Berlin, 1973.

[36] I. NELSON, M.L. BARON, I. SANDLER, Mathematical Models for Geological Materials for Wave-Propagation Studies, appeared in "Shock Waves and the Mechanical Properties of Solids", Syracuse University Press, Syracuse, 1971.

[37] G.C.NAYAK, O.C. ZIENKIEWICZ, Elasto-Plastic stress Analysis. A Generalization for Various Constitutive Relations Including Strain Softening, Int. J.Num. Meth.Eng., Vol. 5, 1972.